Mukesh Kumar[1,2*], Kalpana Chaudhary[1]

J. Electrical Systems 18-4 (2022): 496-519

Regular paper

Bidirectional Converter withCoupled Inductor for High Gain and Low Ripple in PMBLDC Motor for Electric Vehicle Application

This article presents a bidirectional DC-DC converter with a coupled inductor for low input current ripple in step-up operation and low output current ripple in step-down operation for permanent magnet brushless DC (PMBLDC) motor drive based electric vehicle application. PMBLDC motor is deemed more suitable for an EV owing to its high efficiency and torque density. A Bidirectional DC-DC Converter (BDC) is designed and developed for motoring and regenerative braking (RB). In the present work, a BDC is designed to drive a 1 hp PMBLDC motor through a conventional Voltage Source Inverter (VSI). During the converter s step-up operation, EV s load cycle is emulated using a pulley belt setup being driven by a PMBLDC motor. The converter is operating in step-down during RB , the PMBLDC motor is coupled with an inertial load with the help of a belt. Simultaneously, the back Electromotive Force (EMF) of the PMBLDC machine is boosted by using the self-inductance of the PMBLDC motor and the VSI. The braking technique used in this work eliminates the traditional drawback of RB in step-down mode, as the power is extracted even when the motor s back EMF is lower than the voltage of the battery. The control strategy has been implemented by using the TMS320F28335 DSP controller for a developed prototype of the converter and driving the PMBLDC motor. The experimental results are compared to the simulation results and a good alignment has been found.

Keywords: Bidirectional DC-DC Converter, PMBLDC Motor, Coupled Inductor, VSI, Electric Vehicle.

1. Introduction

There are various types of high step-up and down bidirectional DC-DC converters (BDCs) used in electric vehicles (EVs) applications. The voltage amplitude of the battery or fuel cell or super capacitor is low value. The voltage amplitude at which the EV operates at a high value . Therefore, a high gain converter is essential to boost the voltage at which the EV can operate. Another obligatory point for a DC-DC converter is to draw constant current with minimum ripple. Hence, the conjunction of these two objectives shows the important role and thus we proposed topology with high gain and low current ripple. In the past decade, electric vehicles are an alternative option to switch over conventional internal combustion engine (ICE) vehicles. With the enhancement in batteries technology and motors, EVs have become an optimistic substitute for ICE vehicles. Permanent magnet brushless DC (PMBLDC) motor is the most prevailing in the drive train of low to medium power EVs, owing to its high torque density and controllability. In recent years, to improve the drive train's efficiency and driving range, by recovery of energy during regenerative

* Corresponding author: Mukesh Kumar, Indian Institute of Technology (BHU), Varanasi, India E-mail: mukeshk.rs.eee16@iitbhu.ac.in
[1]Indian Institute of Technology (BHU), Varanasi, India
[2] Assistant Professor, Department of Electrical Engineering, Meerut Institute of Engineering and Technology, Meerut, India.

braking (RB) of EV. The electrical system of a power train configuration for EV is shown in Fig. 1, the magnitude and direction of the power are controlled by using the BDC.

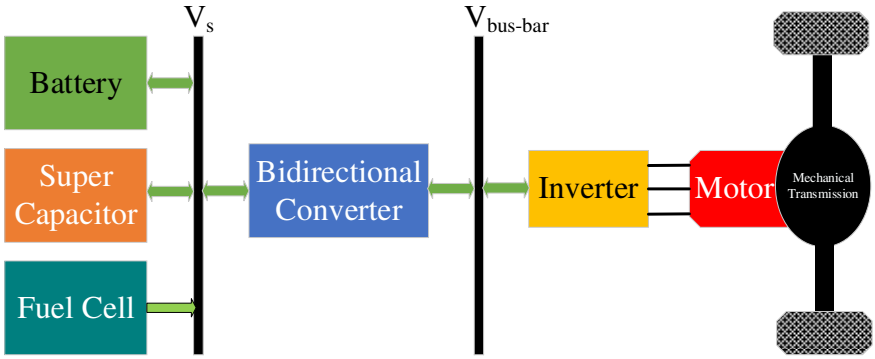

Fig. 1. The electrical system of powertrains.

In the literature, various topologies are available to obtain high voltage gain. There are different types of isolated BDCs [1][2][3], in which a transformer is used to isolate the input and output circuit. But, the transformer leakage inductance and it causes voltage stress on the switches. Different types of non-isolated high gain BDCshave been introduced [4][5]. However, the highest voltage gain is limited by the presence of the circuit parasitic components and the high dutycycle. Besides, its voltage stress on the power switch also limits the high voltage gain. To overcome this problem, various improved transformerless high gain converter [6] has been proposed. In this converter pulse width modulation with 120^o phase shift technique is used. Besides, it also reduces the voltage stresses on power switches. Unfortunately, this technique required a large number of power switches and difficulty in controller design. A cascaded high voltage gain converter [7] is introduced, which has low voltage stress but still needsa large number of power switches. Therefore, a high voltage gain and zero voltage switching (ZVS) BDC [8] with a minimum number of power switches.

There are many different high voltage gain BDCs with multi-input and multi-output ports[9][10] with different input sources and provide different output voltage levels for different applications in EV. The literature study of a novel interleaved non-isolated BDC with a high voltage conversion ratio[11][12][13]. This interleaved converter required a coupled inductor/transformer and ZVS is employed with a phase-shift control technique. The ripple current is remaining to solve. There are different BDC topology derived which has low ripple current as well as high voltage gain [14][15][16]. An active switch-inductor cell is used to make zero ripple current in the converter [16] but it required a large number of components. In recent yearsseveral different topologies with low ripple current and voltage gain are quadratic in nature BDCs [17][18][19] are proposed. All these converters coupled inductor is used and coupled inductor has leakage inductance. The leakage inductance causes additional power losses and hence efficiency decreases.

For step-down or RB application of PMBLDC motor, there are different types of techniques are proposed. A simple and efficient technique for RB is proposed in [20] for brushless DC (BLDC) motor in EV application. The brake force is adopted by fuzzy logic control. In this, during RB the back EMF is boosted by an appropriate switching algorithm.

Another reliable and smooth RB technique is presented in [21] for BLDC motor based on battery/supercapacitor. The brake force distribution is analyzed by the artificial neural network. This has the disadvantage of energy of supercapacitor is not fully utilized because its voltage is higher than the battery voltage.The controlled electrical power is flowing between the battery and the PMBLDC motor. The BDC operates in two modes: Motoring (step-up) and regenerative braking (step-down) mode.

The electrical power transmits from the battery to the PMBLDC motor through VSIin the motoring mode. Simultaneously, the kinetic energy of the PMBLDC motor is converted into electrical energy and fed back to the battery through the bidirectional VSI during the regenerative braking.The proposed topology of the BDC is shown in Fig. 2. A converter with fewer components, in turn having lower losses, is needed to fulfill the requirementof high efficiency and a large voltage gain in EVs. The presented non-isolated BDChas a simple topology, control strategy, and a high voltage gain, which ensures widevoltage range operation compared to conventional BDC.The four switches with anti-parallel diodes have been implemented in this BDC. The number of components can be reduced by using the back diodes of the MOSFETs [22].

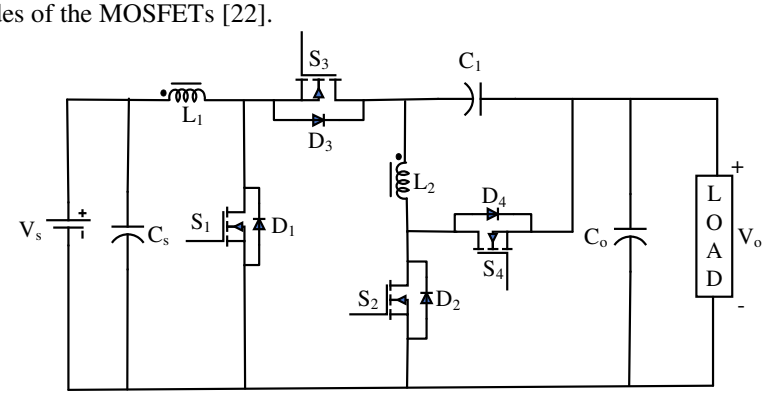

Fig. 2. ProposedConverter.

The main contribution of this work is,

- The converter has high voltage gain and low current ripple.
- Optimum switching technique is employed for operating the converter at reduced switching losses.
- A back EMF boosting technique is used to extract power even at low motor speed.
- Also, the coupled inductor leads the following advantages
  1. By coupling the inductor, the converter has less weight, volume, and cost.
  2. Higher power density.
  3. Efficiency is the same as the conventional quadratic converter.
  4. Due to coupled inductor current ripple is reduced.

The features comparison of different type of bidirectional converter with the proposed converter is shown in Table 1.

Table 1.Features Comparison of the Proposed Converter with the Other Converter.

Topology Features	Conventional	[2]	[3]	[14]	[15]	Proposed Converter
Number of Power Switch	2	9	6	4	4	4
Step-up Voltage Gain	$\frac{D}{(1-D)}$	$\frac{N(1-\sqrt{K_2})}{\sqrt{K_2}(1-2D_2)}$	$\frac{N}{(1-D_1)^2}$	$\frac{2(1-ND)}{1-D}$	$\frac{2+N}{1-D_{boost}}$	$\frac{1}{(1-D)^2}$
Step-down Voltage Gain	D	$\frac{4(1-2D_1)}{NK_1^2}$	$\frac{(1-D_2)^2}{N}$	$\frac{1-D}{2(1-ND)}$	$\frac{D_{buck}}{N+2}$	D^2
Maximum Voltage Stress on Switch	----	----	$\frac{V_L N}{(1-D_1)^2}$	$\frac{V_H(1+N)}{2(1+ND)}$	$\frac{(N+1)V_H}{N+2}$	$\frac{V_s}{(1-D)^2}$
Maximum Efficiency	90 %	96.2 %	94.5 %	96 %	94.2 %	96.5 %

The converter operation in motoring and RB mode are described in this paper. The proposed converter operation in step-up (motoring) modeanalyzed in continuous conduction mode (CCM) and discontinuous conduction mode (DCM) is discussed in section 2 and the step-down (regenerative braking)mode of operation in section 3. The results from simulation and validation through developed prototype are explained in section 4. The conclusion is presented in section 5.

2. Step-up or Motoring Operation

The proposed converter consists of four switches S_1, S_2, S_3, and S_4 with antiparallel diode, capacitor C_1, input and output capacitor C_s, $C_o$respectively, and a coupled inductor which is modelled by magnetizing inductor L_m,leakage inductance L_1 and L_2 in the primary and secondary side. A battery with voltage V_s is connected at the low voltage side, and the DC link or output voltage is V_o. The operation of the proposedconverterisdiscussed in CCM and DCM.

2.1 Step-up in CCM

In step-up operation, the switches S_3 and S_4 are OFF and switchesS_1,S_2 are controlled with a PWM technique to execute the step-up operation.The following two modes can explain the converter's step-up (motoring) operation. The working waveform of the converter is shown in Fig. 4(a)

MODE 1 (t_1, t_2): The switches S_1, S_2 are ON for time intervals 0 to DT_S, and S_3, $S_4$are OFF. In this mode, the energy stored in the capacitor C_1 is transferred to the inductor L_2, so the current in L_2 increasesthe load is supplied through capacitor C_o,while inductor L_1 is being discharged due to negative voltage across it, and its current decreases. The current flowing path of the converter is shown in Fig. 3(a). The voltage across L_1 and L_2 are obtained as follows:

$$V_{L1} = V_s - V_{mp} \quad (1)$$

$$V_{L2} = V_o - V_c - V_{ms} \quad (2)$$

$$i_c = i_{L2} \quad (3)$$

$$i_{co} = i_c + i_o \quad (4)$$

Where V_{mp}, V_{ms} is the amount of voltage across L_m in the primary and secondary sides of the coupled inductor.

MODE II (t_2, t_3): In this mode, all the switches S_1, S_2 S_3, S_4 are OFF, and the diode D_3 and D_4 are forward biased for a time interval (1-D)T_s. During this mode, the inductor L_2 is transferring its stored energy to the DC link capacitor $C_o$and load and capacitor C_1 inductor $L_1$is charged by voltage source V_s. The current flowing path of the converter is shown in Fig. 3(b).Current in inductor L_1 is increases and L_2 current decreases. The voltage across L_1 and L_2 are obtained as follows:

$$V_{L1} = V_s + V_c - V_{mp} - V_o \quad (5)$$

$$V_{L2} = -V_c - V_{ms} \quad (6)$$

$$i_c = -i_{L1} + i_{L2} \quad (7)$$

$$i_{co} = i_{L1} - i_o \quad (8)$$

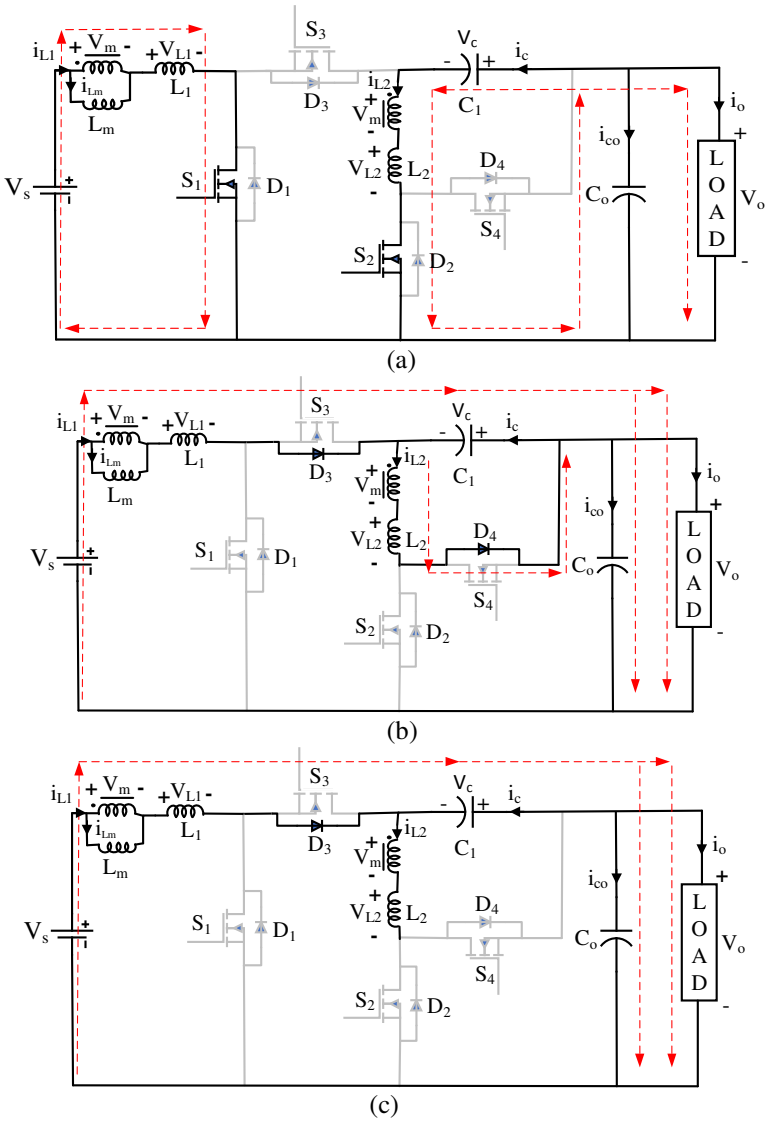

Fig. 3. Converter's step-up operation in (a) Mode I (b) Mode II (c) Mode III (DCM).

Now by applying the volt-sec balance principle on inductors L_1 and L_2 the following equation is obtained:

$$DV_s - DV_{mp} + (1-D)(V_s + V_c - V_{mp} - V_o) = 0 \quad \textbf{(9)}$$

$$DV_o - DV_c - DV_{ms} + (1-D)(-V_c - V_{ms}) = 0 \quad \textbf{(10)}$$

where, D is the duty ratio, on solving these two equations the voltage gain in step-up operation is obtained as:

$$G_{step-up} = \frac{V_o}{V_s} = \frac{1}{(1-D)^2} \tag{11}$$

The voltage across capacitor C_1 is obtained as:

$$V_c = \frac{V_s}{(1-D)} \tag{12}$$

From (11), the $G_{step-up}$ is independent of the turns ratio of the coupled inductor. So that the V_{mp} and V_{ms} are considered equal, and it is denoted as V_m.

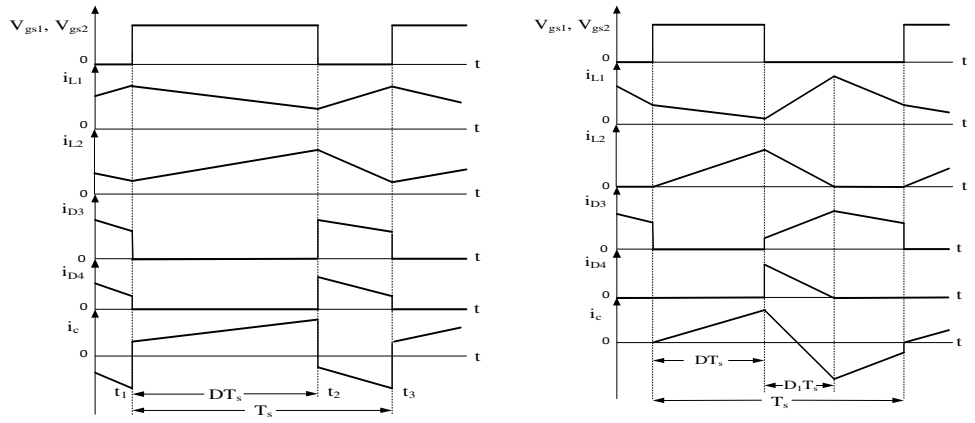

(a) (b)

Fig. 4. Typicalwaveforms of the converter in step-up operation (a) CCM (b) DCM

After that, by applying the Ampere-second balance principle on capacitor C_1 and C_o the following equation are obtained:

$$DI_{L2} + (1-D)(I_{L1} - I_{L2}) = 0 \tag{13}$$

$$DI_c + DI_o + (1-D)(I_{L1} - I_{L2}) = 0 \tag{14}$$

On solving the abovementioned equation, the average inductor current I_{L1} and I_{L2} are obtained:

$$I_{L1} = \frac{I_o}{(1-D)^2} \tag{15}$$

$$I_{L2} = \frac{I_o}{(1-D)} \tag{16}$$

Where I_o average load current in step-up operation. The load on the converter consists of a PMBLDC motor which is fed through a voltage source inverter. A pulley is connected to the shaft of the motor, load torque is applied on the pulley through the belt, both ends of the belt are connected with electronics weighing instrument.

From Fig. 4(a), the current ripples of the inductor are calculated by applying voltage equation across the inductor in time interval t_1 to t_2 of step-up operation as follows:

$$L_1 \frac{di_{L1}}{dt} + L_m \left(\frac{di_{L1}}{dt} + \frac{di_{L2}}{dt}\right) = V_s \tag{17}$$

$$L_2 \frac{di_{L2}}{dt} + L_m \left(\frac{di_{L1}}{dt} + \frac{di_{L2}}{dt}\right) = V_o - V_c \tag{18}$$

On solving (17), (18) the current ripple of inductor L_1 (Δi_{L1}) and L_2 (Δi_{L2}) are obtained:

$$\Delta i_{L1} = \frac{V_s D T_s [L_2(1-D) - D L_m]}{L(1-D)} \tag{19}$$

$$\Delta i_{L2} = \frac{V_s D T_s [L_1 + D L_m]}{L(1-D)} \tag{20}$$

$$L = L_1 L_2 + L_1 L_m + L_2 L_m \tag{21}$$

2.2 Step-up in DCM

The proposed converter operates in the DCM when i_{L2} is discontinuous. The voltage and current waveforms of the converter are shown in Fig. 4(b).

Mode I (t_1, t_2): In this mode, the working of the converter is alike to Mode I of the CCM. The voltage across L_1, L_2, and current in capacitor C_1 and C_o are similar to the first mode of CCM.

Mode II (t_2, t_3): In this mode, S_1 and S_2 are turned OFF and diode D_3 and D_4 are forward biased. The capacitor $C_1$and inductor $L_2$are discharged to the load and also capacitor Co charged. The current through inductor L1 is increased because the voltage

across it is positive. The voltage across inductor L_1 and $L_2$and current through capacitor C_1 and C_o are written as

$$V_{L1} = V_o + V_c + V_s - V_{mp} \quad (22)$$

$$V_{L2} = -(V_{ms} - V_c) \quad (23)$$

$$i_c = i_{L2} - i_{L1} \quad (24)$$

$$i_{co} = i_{L1} - i_o \quad (25)$$

Mode III (t_3, t_4): In this mode, switches S_1 and S_2 are remain turned OFF. As the inductor L_2 current is zero, the diode D_4 is OFF and diode D_3 remains turned ON and the L_1 current is flowing. In this mode, the L_1 is discharged into the capacitor C_1. As inductor L_2 current is zero, C_o supplies the load in this mode. The voltage across inductor L_1 and L_2 and current through capacitor C_1 and C_o are written as

$$V_{L1} = V_o + V_c + V_s - V_{mp} \quad (26)$$

$$V_{L2} = 0 \quad (27)$$

$$i_c = -i_{L1} \quad (28)$$

$$i_{co} = i_{L1} - i_o \quad (29)$$

As the average current of D_4 is equal to I_o, substituting (19) into (17). Then the voltage gain of the converter in DCM is obtained as

$$\frac{V_o}{V_s} = \frac{D[D_1 L(1-D) - DL_2(L_1 + L_m)(1-D) - D^2 L_m(L_1 + L_m)]}{KL(1-D)} \quad (30)$$

where $K= 2L/R_oT_S$

From Fig 4(b) D_1 duty cycle of mode II . D_1 is calculated by equalizing (20) equal to the amount of Δi_{L2} in mode II.

$$D_1 = \frac{L_2(L_1 + DL_m)}{L} \tag{31}$$

According to the basic principle, if Δi_{Lm}= 0, then inducted voltage is zero and the converter will not work. So that, there should be minimum ripple current by selecting a proper value of inductors. The ripple current in magnetizing inductor L_m is the sum of ripple current in L_1 and L_2, therefore the ripple current is obtained as

$$\Delta i_{Lm} = \Delta i_s = \Delta i_{L1} + \Delta i_{L2} \tag{32}$$

$$L_m = \frac{V_s DT_s[L_1 + L_2(1-D)] - L_1 L_2(1-D)\Delta i_s}{\Delta i_s(1-D)(L_1 + L_2)} \tag{33}$$

The inductors' values can be selected as per the permissible current's ripple in (19), (20), and (33). Because getting the exact leakage inductances L_1 and L_2 are difficult, auxiliary inductors are connected in a series of either side of the coupled inductor to get calculated current ripple.

3. Step-down or Regenerative braking Operation

For RB operation there should be a reversal of energy flow. To reverse the energy flow, the PMBLDC motor should act as a generator. The stored energy in the inertial flywheel is fed back to the battery by stepping down the voltage label to the source voltage label with the help of a bidirectional converter. In step-down or RB operation of the converter, the switches S_1, S_2 are OFF and S_3, S_4 are controlled by the PWM technique to perform step-down or RB operation. The following two modes explain the converter's step-down or RB operation.

3.1 Step-down in CCM

MODE 1 (t_1,t_2): In this mode, the switches S_3, S_4 are ON, and the remaining two switches are OFF for the time of DTs. The inductor L_2, capacitor $C_1$is energized through source voltage V_s, and $L_1$is supplied to the load and C_s. The current in L1 decreases and L2 current increases. Some of the current and voltage waveforms are illustrated in Fig. 6(a). Fig. 5(a) shows the current flowing path in the circuit in this mode.
The voltage across L_1 and L_2 and current through capacitor C and C_s are obtained as follows:

$$V_{L1} = V_s - V_c - V_{mp} - V_o \tag{34}$$

$$V_{L2} = V_c - V_{ms} \quad (35)$$

$$i_c = i_{L1} - i_{L2} \quad (36)$$

$$i_{cs} = i_{L1} - i_o \quad (37)$$

Where V_{mp}, V_{ms} is the amount of voltage developed in the primary and secondary sides of the coupled inductor.

MODE 2 (t_2, t_3): In this mode, all the switches S_1, S_2, S_3, S_4 are OFF and diode D_1 and D_2 are forward biased for a time interval (1-D)T_s. During this mode, the energy stored in inductor L_2 is transferred to capacitor C_1, the load is supplied by capacitor Cs, and inductor L_1 is being charged due to positive voltage across it. The current flowing path in the circuit is shown in Fig. 5(b).

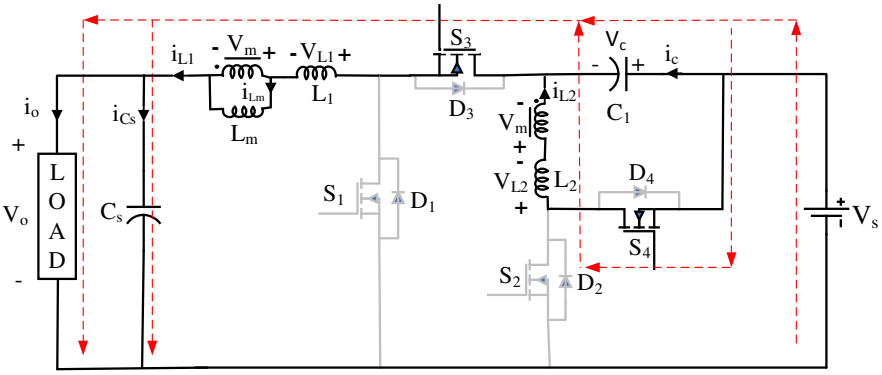

(a)

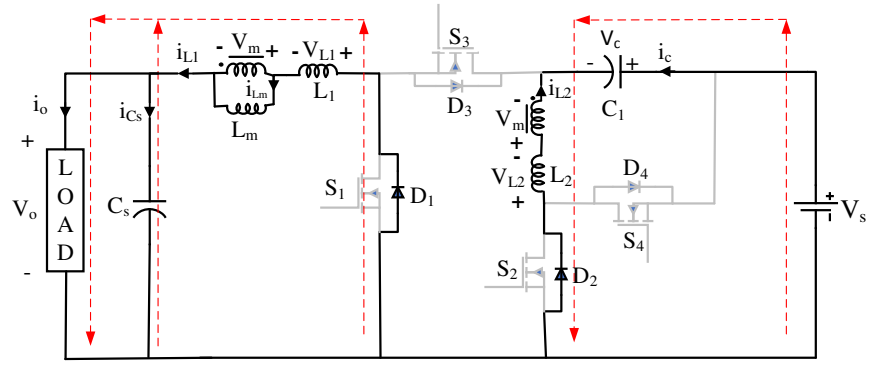

(b)

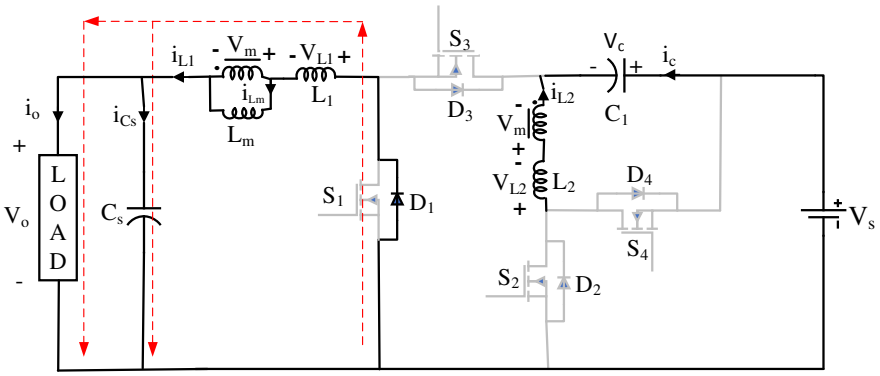

(c)

Fig. 5. Converter's step-down operation in (a) Mode I (b) Mode II (c) mode III (DCM).

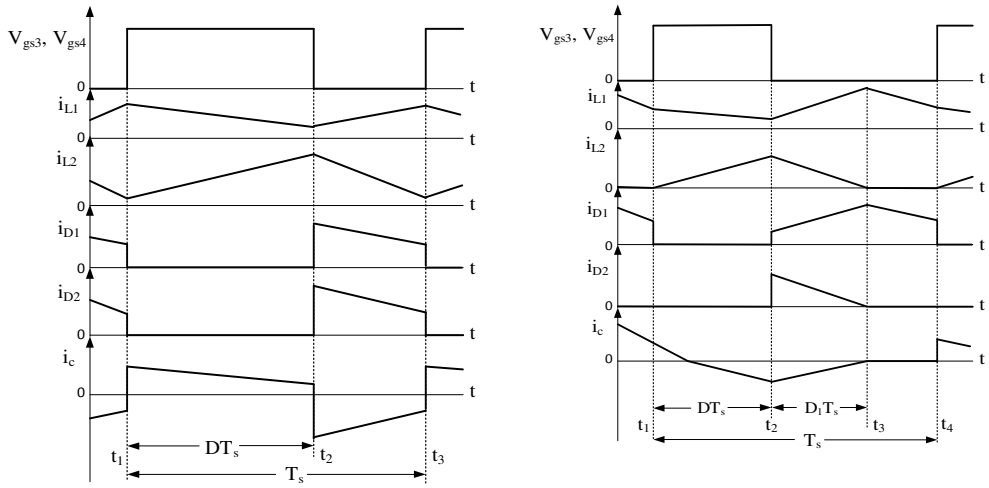

(a) (b)

Fig. 6. Key waveforms of the converter in step-down operation (a) CCM (b) DCM.

The voltage across L_1 and L_2 and current through capacitor C and C_s are obtained as follows:

$$V_{L1} = V_o - V_{mp} \quad \textbf{(38)}$$

$$V_{L2} = V_c - V_s - V_{ms} \quad \textbf{(39)}$$

$$i_c = -i_{L2} \quad \textbf{(40)}$$

(41)

$$i_{cs} = i_{L1} - i_o$$

Now by applying the volt-sec balance principle on inductors L_1 and L_2 the following equation is obtained:

(42)

$$D(V_s - V_c - V_{mp} - V_o) + (1 - D)(V_o - V_{mp}) = 0$$

(43)

$$DV_c - DV_{ms} + (1 - D)(V_c - V_s - V_{ms}) = 0$$

On solving (30) and (31), the voltage gain in step-down operation is obtained as:

(44)

$$M_{step-down} = \frac{V_o}{V_s} = D^2$$

The voltage across capacitor C_1 is calculated as:

(45)

$$V_C = DV_s$$

From (32), voltage gain $M_{step-down}$ is independent of the turns ratio of the coupled inductor. So that the V_{mp} and V_{ms} are considered equal, and it is denoted as V_m. After that, by applying the Ampere-second balance principle on capacitor C_1 and C_s the following equation is obtained:

(46)

$$D(I_{L1} - I_{L2}) - (1 - D)I_{L2} = 0$$

(47)

$$DI_{L1} + DI_o + (1 - D)(I_o - I_{L1}) = 0$$

On solving the abovementioned equation, the average inductor current I_{L1} and I_{L2} are obtained:

(48)

$$I_{L1} = I_o$$

(49)

$$I_{L2} = DI_o$$

From Fig. 8, the current ripples of the inductor are calculated by applying voltage equation across the inductor in time interval t_1 to t_2 of step-down operation as follows:

(50)

$$L_1 \frac{dI_{L1}}{dt} + L_m \left(\frac{dI_{L1}}{dt} + \frac{dI_{L2}}{dt}\right) = V_s - V_c - V_o$$

$$L_2 \frac{di_{L2}}{dt} + L_m \left(\frac{di_{L1}}{dt} + \frac{di_{L2}}{dt} \right) = V_c \quad (51)$$

On solving (38), (39) the current ripple of inductor L_1 (Δi_{L1}) and L_2 (Δi_{L2}) are obtained:

$$\Delta i_{L1} = \frac{V_s D T_s [L_2(1 - D - D^2) - L_m(1 - D)^2]}{L} \quad (52)$$

$$\Delta i_{L2} = \frac{V_s D T_s [L_1 - D L_m (1 - D)]}{L} \quad (53)$$

3.2 Step-down in DCM

The converter operates in DCM when in duct or L_2 current is discontinuous. The typical current and voltage waveform of the converter in DCM is shown in Fig. 6(b).

Mode I (t_1, t_2): In this mode, the working of the converter is alike to Mode I step-down in CCM operation.

Mode II (t_2, t_3): The switch S_3 and S_4 are turned OFF and the diode D_1 and D_2 are forward biased for time interval D_1T_s. In this mode energy stored in inductor L_2istransferred to capacitor C_1 and inductor L_1isbeingcharged due to positive voltage a cross it.

Mode III (t_3, t_4): In this mode, the switch S_3 and S_4 are still turned OFF. As the inductor L_2currentiszero, diode D_2 is OFF and diode D_1remainsturned ON and inductor L_2currentiscontinuous. The current flowing path of the circuit is shown in Fig. 5(c). The voltage a cross inductors L_1 and L_2 and current in capacitors C_1 and C_S in this interval are written as

$$V_{L1} = -(V_m + V_o) \quad (54)$$

$$i_{cs} = i_{L1} - i_o \quad (55)$$

Since, the average current of D_1(I_{D1}) is equal to the average input current, by substituting (53) into (51), V_{L2}iscalculated in Mode II, then the voltage gain in DCM is obtained as

$$\frac{V_o}{V_s} = \frac{D_1^2[(L_1 + L_m)(1 - D)]}{KD^2 + D_1^2} \quad (56)$$

From Fig. 6(b), D_1isthe duty cycle of mode II and it is calculated by equalizing (53) equal to the amount of Δi_{L2} in mode II.

$$D_1 = \frac{L_1[L_2 + D L_m (L_1 + L_m)]}{L} \quad (57)$$

The ripple current in magnetizing current is equal to the sum of ripple currents in L_1 and L_2whichisequal to the output ripple current.

$$\Delta i_{Lm} = \Delta i_o = \Delta i_{L1} + \Delta i_{L2} \quad (58)$$

$$L_m = \frac{L_1 + L_2(1 - D - D^2) - L_m(1 - D)[DL_m + (1 - D)] - L_1 L_2 \Delta i_o}{\Delta i_o (L_1 + L_2)} \quad (59)$$

The inductors' values are selected according to the permissible currents' ripple in (50), (51), and (59).

3.3 VSI Control for Regenerative Braking:

RB can be achieved by reversal of power flow in the circuit with an appropriate switching strategy, during RB the motor act as a generator and kinetic energy is transferred to the battery. The simple and efficient method to control the PWM employed RB. However, at the low speed of the PMBLDC motor, back EMF is not enough to battery voltage. Therefore the recovery of energy cannot take place. To make energy recovery, the back-EMF voltage has to boost up to dc bus voltage with the help of self-inductance of the motor. Turn off all switches on the upper side of the VSI and control the switches on the lower side of the VSI with PWM. Fig. 7 shows the back EMF, armature current, and switching signals for the VSI, in which only one switch operated in each commutation state. By controlling the switch, the whole circuit mold into a boost circuit. The equivalent circuit of each commutation state is shown in Fig. 8.

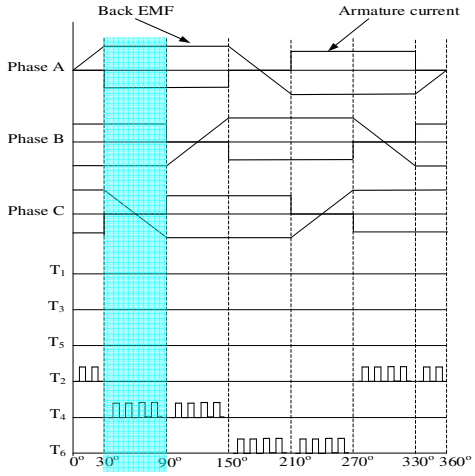

Fig. 7. The waveform of PMBLDC motor with the control signal during RB.

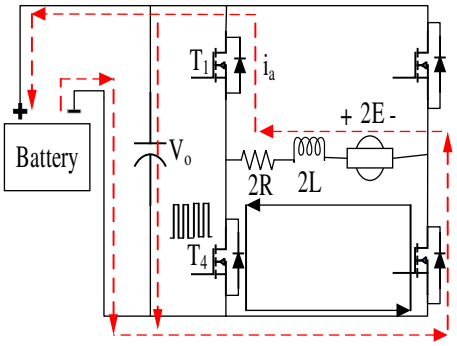

Fig. 8. Equivalent circuit of VSI during RB.

4. Simulation and Experimental Results

4.1 Simulation Results

The proposed converter and VSI for the PMBLDC motor are simulated using MATLAB/Simulink. The load on the motor is applied through the pulley and belt during motoring and an inertial load of 0.1 kg-m2 during RB operation. The parameters of the PMBLDC are given in Table 1. The proposed converter is simulated and designed for 1 Kw

with battery voltage V_S=48 V, output voltage V_0= 200 V, and switching frequency of 40 kHz. The converter parameters are chosen to operate in CCM for step-up and step-down are given in Table 2.The converter and inverter switching PWM generated in MATLAB/Simulink is illustrated in Fig. 9. The steady-state inductor's current in the step-up operation of the converter is illustrated in Fig. 10. One can see, when the switch is ON then the inductor L_1 current is decreases, and the inductor L_2 current increases.

Table 2. PMBLDC Motor Parameters

Parameter	Value
Rated Power	1.1 hp
Per Phase Resistance (Ra)	1.09 Ω
Per Phase Inductance (La)	3.37 mH
Voltage Constant K	51.3 V/krpm
Inertia (J)	0.00014 kg-m2
Pole Pair (P)	2

Table 3. Proposed Converter Parameters

Parameter	Value
Power	1000 W
Output voltage	200 V
Switching Frequency	40 kHz
Magnetizing Inductance (Lm)	480 µH
Leakage inductance L_1= L_2	96 µH
Capacitor C_S, C_1, C_o	100 µF, 47µF, 220 µF

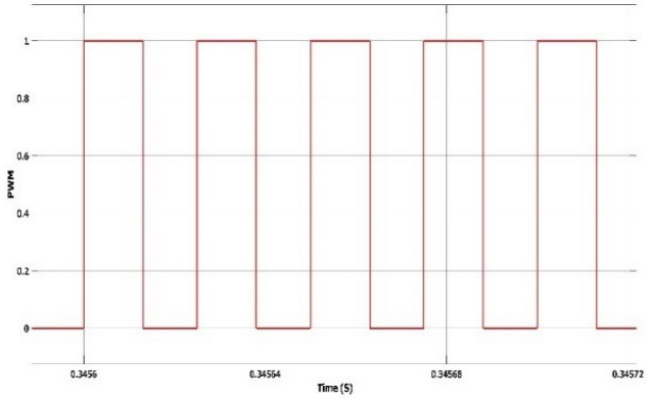

(a)

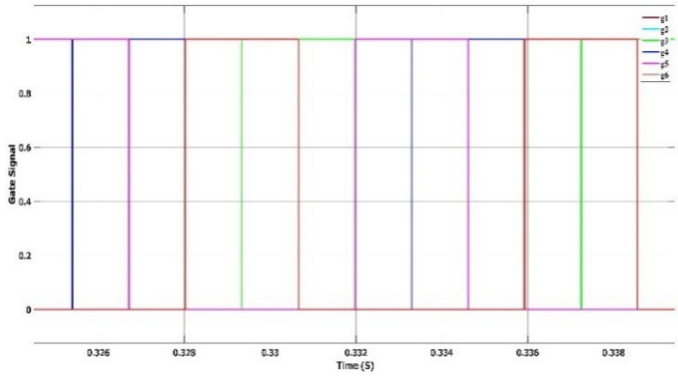

(b)

Fig. 9. The switching PWM signal for (a) Converter (b) Inverter.

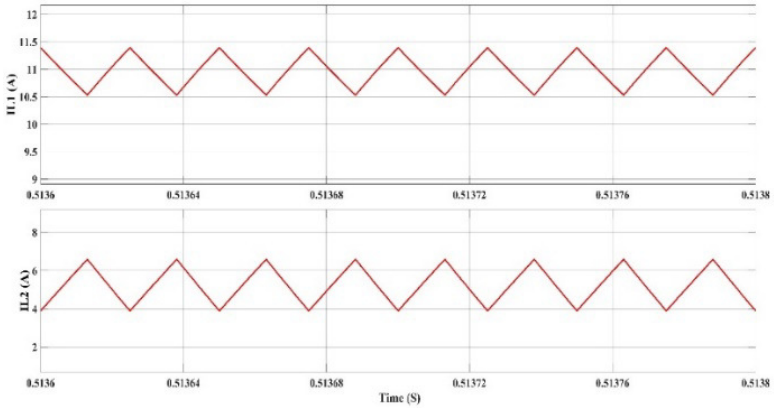

Fig. 10. Steady-state inductor L_1 and L_2 current during converter's step-up operation.

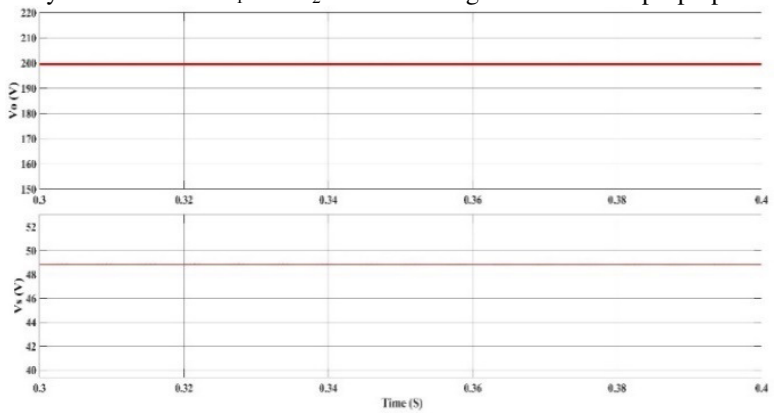

Fig. 11. Steady-state input and output voltage during converter's step-up operation

The converter output voltage and battery voltage waveform during the converter's step-up operation are shown in Fig. 11. One can see the output voltage of 200 V and battery voltage of 48 V in Fig. 11. The voltage stress on switch S_1 and S_4 during step-up operation of the converter is shown in Fig. 12.

The converter is operated in a voltage control close loop to get desired output voltage. The voltage and current waveform in a closed-loop when load torque is changed on the

PMBLDC motor are illustrated in Fig. 13. One can see that at time t=0.4 sec load torque is increased then there is a small dip in output voltage for a few milliseconds and then the controller has maintained the output voltage of 200 V by controlling the duty cycle of the converter and inductor's current also increased to meed the load.

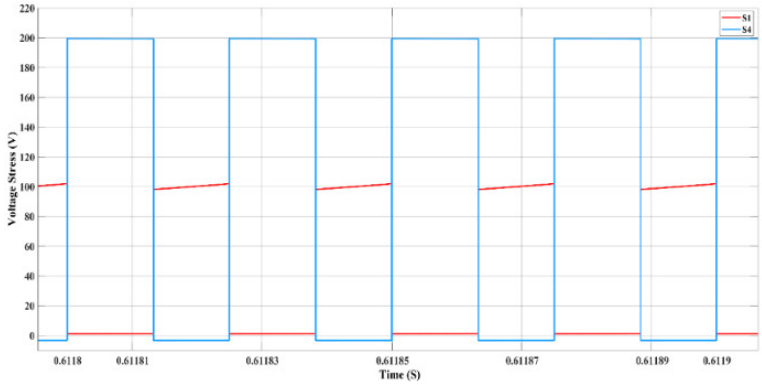

Fig. 12. Voltage stress on switch S_1 and S_4 in step-up operation of converter.

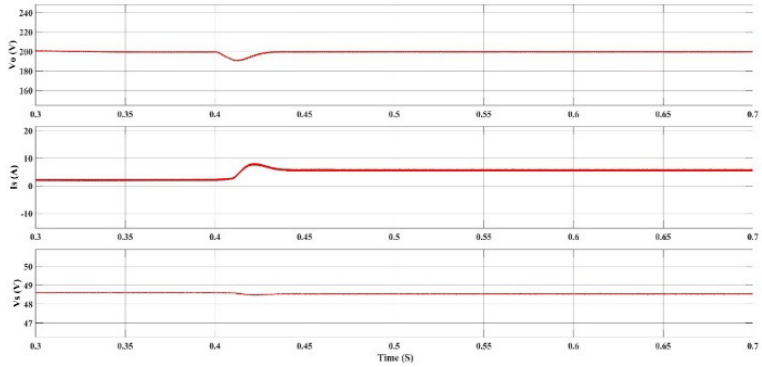

Fig. 13. Input and output voltage and inductor's current waveform in close loop

When regenerative braking is applied to EV, the PMBLDC motor act as a generator, and the back EMF of the motor is boosted up to extract the maximum energy stored in the inertial flywheel even at low rotor speed and fed back to the battery by stepping down the voltage to battery level voltage. During RB the proposed converter operates in step-down mode. The steady-state output and input voltage during step-down operation of the converter are shown in Fig. 14.The steady-state inductor's current during step-down operation of the converter is shown in Fig. 15.

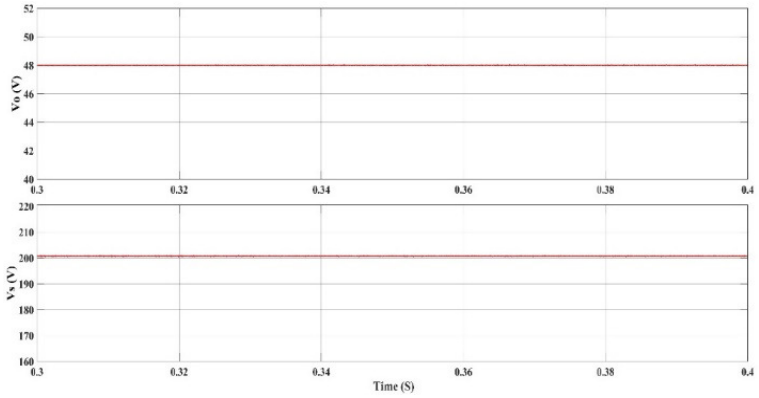

Fig. 14. Steady-state output and input voltage during step-down operation of the converter.

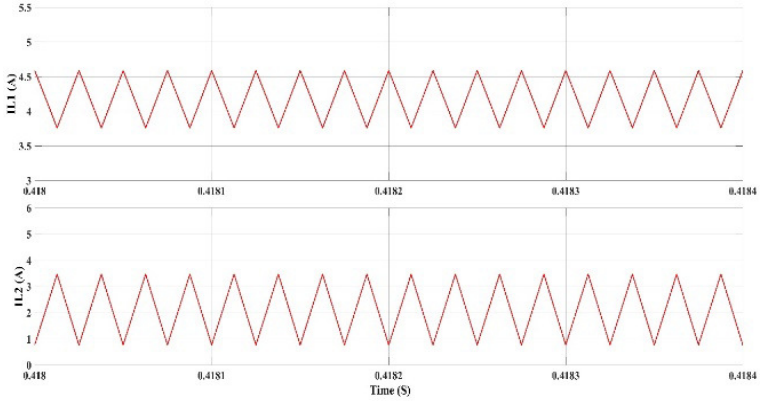

Fig. 15. Steady-state inductor's current during step-down operation of the converter.

4.2 Experimental Results

The prototype of the proposed converter is designed and developed in the laboratory for experimental validation. Fig. 16 shows the hardware setup of the converter. The Lithium-ion battery is connected to the input of the converter, the output of the converter is connected to the VSI, PMBLDC motor is connected through VSI and a pulley belt arrangement. The PWM signal for converter and VSI are generated by the TMS320F28335 DSP controller. The load torque is applied through the belt on the pulley during the step-up operation of the converter. Fig. 17 shows the steady-state output voltage, battery voltage, and inductor's current in step-up operation.

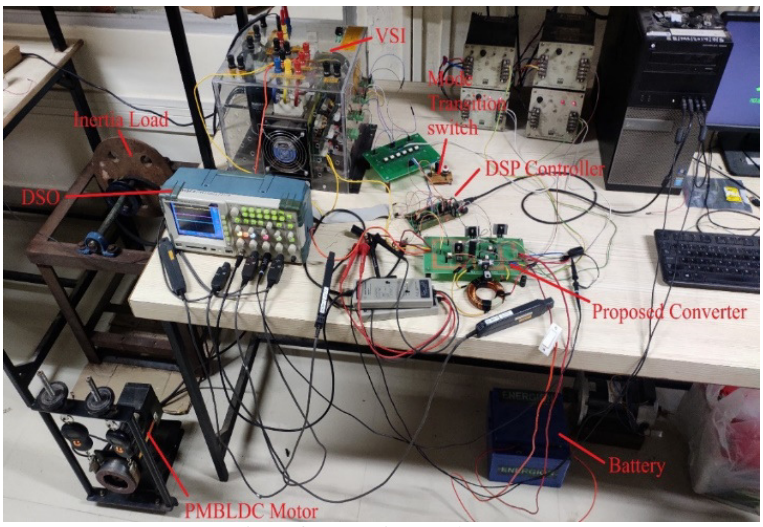

Fig. 16. Experimental setup.

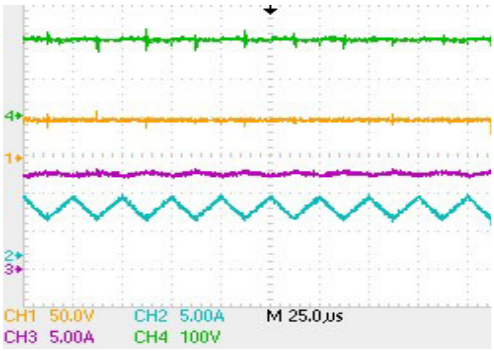

Fig. 17. Steady-state output voltage V_o (channel 4), input voltage V_s (channel 1), I_{L1} (channel 3), and I_{L2} (channel 2) in step-up operation of the converter.

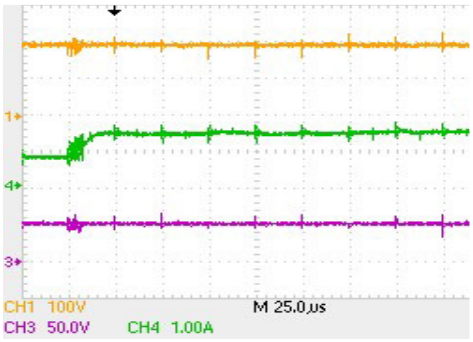

Fig. 18. V_o (channel 1), i_{L1} (channel 2), i_{L2} (channel 4), and PWM of S_1 and S_2 (channel 3) in step-up operation of the converter.

When a sudden increase in the load, the converter, there is an increase in load current, and the output voltage is maintained at 200 V by the controller. Fig. 18 shows the output voltage, inductor currents and switching PWM of switches S_1 and S_2. One can see that when switches S_1 and S_2 are ON the inductor current i_{L1} decreases and inductor current i_{L2} increases. Fig. 19 shows the output voltage, input voltage, and load current when a sudden load is increased. From Fig. 18 it can say that the PI controller is working satisfactorily to maintain the output voltage whenever there is a change in load on the converter. Fig. 20 shows the voltage stress on switches S_1 and S_2 during the step-up operation of the converter.

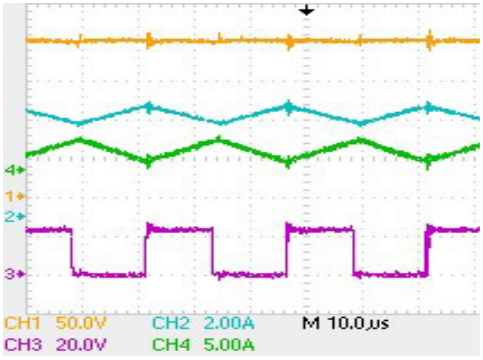

Fig. 19. V_s (channel 3), V_o (channel 1) and load current (channel 4) when sudden load is increased during step-up operation of the converter.

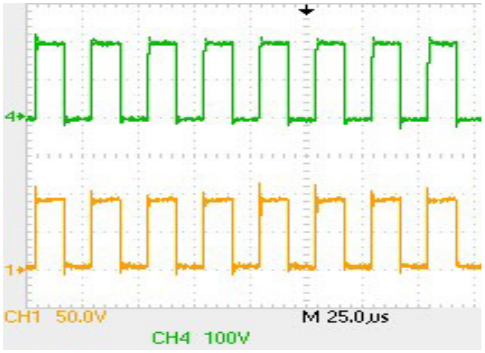

Fig. 20. The voltage stress on S_1 (channel 10) and S_2 (channel 4) during step-up operation of the converter.

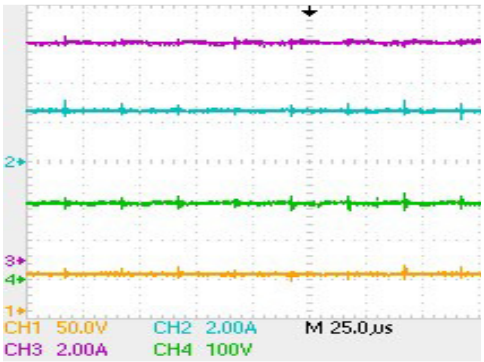

Fig. 21. Steady-state V_o (channel 4), output current (channel 2), V_s (channel 1), and input current (channel 3) in step-up operation of the converter.

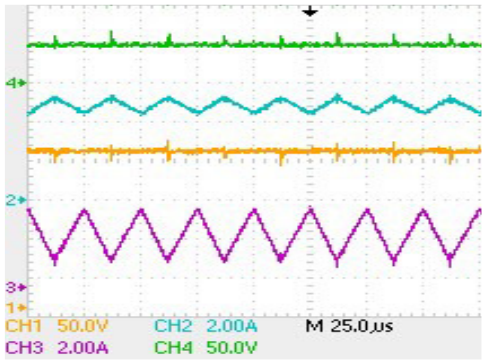

Fig. 22. Steady-stateV_o (channel 4), V_s (channel 1), I_{L1} (channel 2), and I_{L2} (channel 3) in step-down operation of the converter.

The steady-state output voltage, output current, input voltage, and input current during step-up operation of the converter are shown in Fig. 21. To show the RB operation, the PMBLDC motor is coupled with an inertial load through the belt. When RB is applied, PMBLDC motor will act as generator and energy extracted from the stored kinetic energy in inertial load and fed back to the battery by stepping down the voltage level to battery level through the converter. During RB, the converter will act as a step-down operation. The steady-state inductor currents, input, and output voltage during RB are

Shown in Fig 22 . The output voltage, inductor currents, and switching PWM of switches S3 and S4 during step-down operation of the converter are shown in Fig. 23. One can see that, when switches S_3 and S_4 are ON the inductor current i_{L1} decrease and inductor current i_{L2} increases.

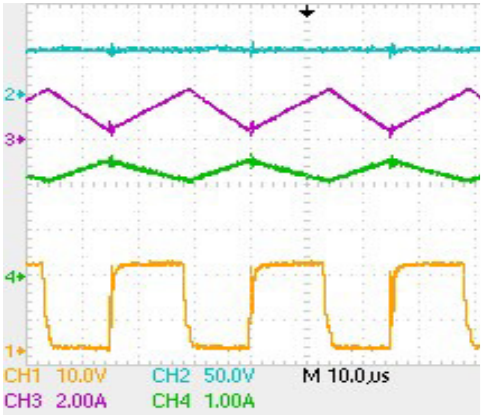

Fig. 23. V_o (channel 2), i_{L1} (channel 4), i_{L2} (channel 3), and PWM of switches S_3 and S_4 (channel 1) in step-down operation of converter.

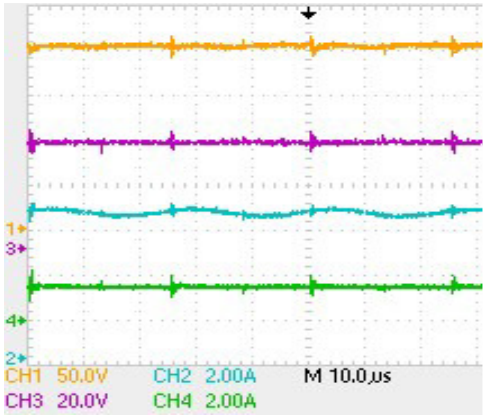

Fig. 24. V_o (channel 3), output current (channel 2), V_s (channel 1), and input current (channel 4) in step-down operation of the converter.

The steady-state output voltage, output current, input voltage, and input current during step-up operation of the converter are shown in Fig. 24. When a sudden increase in load, the closed-loop voltage control of output voltage, output current and input voltage are shown in Fig. 25. From Fig. 25, one can say that the load on converter is changes but output voltage is maintained at 48 V by controller.

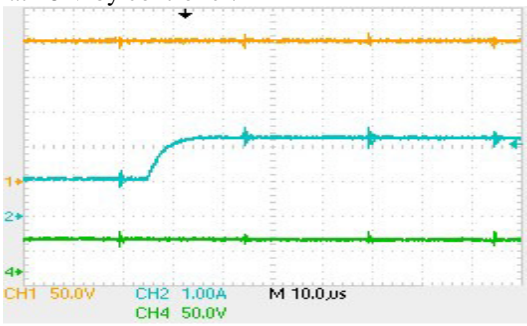

Fig. 25. Closed-loop output voltage (channel 4), output current (channel 2), and input voltage (channel 1) in step-down operation of the converter.

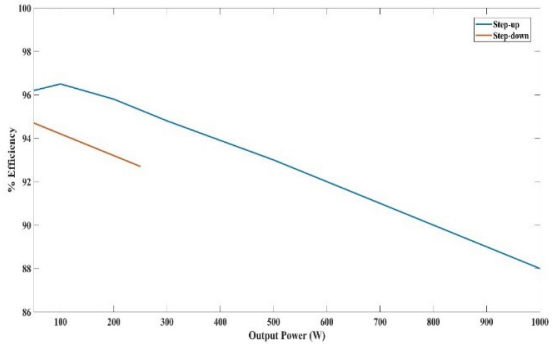

Fig. 26. Efficiency curve of the converter in step-up and step-down operation.

The efficiency curve of the converter in step-up and step-down operations is illustrated in Fig. 26 . The converter maximum efficiency of 96.5% and 94.6% in step-up and down operation, respectively.

Conclusion

The proposed converter is designed, developed in the laboratory, and tested on PMBLDC motor in motoring and regenerative braking mode for EV application. The proposed converter operation in CCM and DCM for step-up and step-down modes was discussed. The voltage gain in step-up mode was similar to the conventional cascaded boost converter. Also, the voltage gain in step-down mode was similar to the conventional cascaded buck converter. However, a coupled inductor with pertinent windings and proper switching control, input and output current ripples were minimized in step-up and step-down modes, respectively. The energy flow direction is controlled by operating the mode transition switch to change the working of the bidirectional DC-DC converter and VSI. The proposed converter could attain high voltage gain with low current ripple at all operating points. The control technique of the VSI using self-inductance of the motor for boosting back EMF of the PMBLDC motor is implemented. The implemented control strategy and system configuration are economical and efficient for EV applications.

References

[1] T. Liang, S. Member, and J. Lee, "Novel High-Conversion-Ratio High-Efficiency Isolated Bidirectional DC – DC Converter," vol. 62, no. 7, pp. 4492–4503, 2015.

[2] J. Lu, Y. Wang, X. Li, and C. Du, "High-Conversion-Ratio Isolated Bidirectional DC-DC Converter for Distributed Energy Storage Systems," *IEEE Trans. Power Electron.*, vol. 34, no. 8, pp. 7256–7277, 2019, doi: 10.1109/TPEL.2018.2881085.

[3] Y.-E. Wu and Y.-T. Ke, "A Novel Bidirectional Isolated DC-DC Converter With High Voltage Gain and Wide Input Voltage," *IEEE Trans. Power Electron.*, vol. 36, no. 7, pp. 7973–7985, 2021, doi: 10.1109/TPEL.2020.3045986.

[4] A. Rodríguez-lorente, A. Barrado, S. Member, C. Calderón, C. Fernández, and A. Lázaro, "Non-inverting and Non-isolated Magnetically Coupled Buck – Boost Bidirectional," vol. 35, no. 11, pp. 11942–11954, 2020.

[5] B. Chandrasekar *et al.*, "Non-Isolated High-Gain Triple Port DC–DC Buck-Boost Converter With Positive Output Voltage for Photovoltaic Applications," *IEEE Access*, vol. 8, pp. 113649–113666, 2020, doi: 10.1109/ACCESS.2020.3003192.

[6] Z. Saadatizadeh, P. C. Heris, M. Sabahi, and E. Babaei, "A DC-DC Transformerless High Voltage Gain Converter with Low Voltage Stresses on Switches and Diodes," *IEEE Trans. Power Electron.*, vol. 34, no. 11, pp. 10600–10609, 2019, doi: 10.1109/TPEL.2019.2900212.

[7] J. Chen, D. Sha, Y. Yan, B. Liu, and X. Liao, "Cascaded High Voltage Conversion Ratio Bidirectional Nonisolated DC-DC Converter with Variable Switching Frequency," *IEEE Trans. Power Electron.*, vol. 33, no. 2, pp. 1399–1409, 2018, doi: 10.1109/TPEL.2017.2679105.

[8] M. Aamir, S. Mekhilef, and H. J. Kim, "High-Gain Zero-Voltage Switching Bidirectional Converter With a Reduced Number of Switches," *IEEE Trans. Circuits Syst. II Express Briefs*, vol. 62, no. 8, pp. 816–820, 2015, doi: 10.1109/TCSII.2015.2433351.

[9] C. M. Lai, Y. H. Cheng, M. H. Hsieh, and Y. C. Lin, "Development of a Bidirectional DC/DC Converter with Dual-Battery Energy Storage for Hybrid Electric Vehicle System," *IEEE Trans. Veh. Technol.*, vol. 67, no. 2, pp. 1036–

1052, 2018, doi: 10.1109/TVT.2017.2763157.

[10] B. Zhu, H. Hu, H. Wang, and Y. Li, "A Multi-Input-Port Bidirectional DC/DC Converter for DC Microgrid Energy Storage System Applications," *Energies*, vol. 13, no. 11, 2020, doi: 10.3390/en13112810.

[11] C. L. Shen, H. Liou, T. C. Liang, and H. Z. Gong, "An Isolated Bidirectional Interleaved Converter with Minimum Active Switches and High Conversion Ratio," *IEEE Trans. Ind. Electron.*, vol. 65, no. 3, pp. 2313–2321, 2018, doi: 10.1109/TIE.2017.2745441.

[12] M. Pajnić and P. Pejović, "Zero-Voltage Switching Control of an Interleaved Bi-Directional Buck-Boost Converter with Variable Coupled Inductor," *IEEE Trans. Power Electron.*, vol. 34, no. 10, pp. 9562–9572, 2019, doi: 10.1109/TPEL.2019.2893703.

[13] Y. Zhang, W. Zhang, F. Gao, S. Gao, and D. J. Rogers, "A Switched-Capacitor Interleaved Bidirectional Converter with Wide Voltage-Gain Range for Super Capacitors in EVs," *IEEE Trans. Power Electron.*, vol. 35, no. 2, pp. 1536–1547, 2020, doi: 10.1109/TPEL.2019.2921585.

[14] E. Babaei, Z. Saadatizadeh, and V. Ranjbarizad, "A new nonisolated bidirectional DC-DC converter with ripple-free input current at low-voltage side and high conversion ratio," *Int. Trans. Electr. Energy Syst.*, vol. 28, no. 2, pp. 1–21, 2018, doi: 10.1002/etep.2494.

[15] Y. Zhang, H. Liu, J. Li, and M. Sumner, "A Low-Current Ripple and Wide Voltage-Gain Range Bidirectional DC-DC Converter with Coupled Inductor," *IEEE Trans. Power Electron.*, vol. 35, no. 2, pp. 1525–1535, 2020, doi: 10.1109/TPEL.2019.2921570.

[16] Z. Wang, P. Wang, B. Li, X. Ma, and P. Wang, "A Bidirectional DC–DC Converter With High Voltage Conversion Ratio and Zero Ripple Current for Battery Energy Storage System," *IEEE Trans. Power Electron.*, vol. 36, no. 7, pp. 8012–8027, 2021, doi: 10.1109/TPEL.2020.3048043.

[17] V. F. Pires, D. Foito, and A. Cordeiro, "A DC-DC Converter with Quadratic Gain and Bidirectional Capability for Batteries/Supercapacitors," *IEEE Trans. Ind. Appl.*, vol. 54, no. 1, pp. 274–285, 2018, doi: 10.1109/TIA.2017.2748926.

[18] S. Lee and H. Do, "Quadratic Boost DC–DC Converter With High Voltage Gain and Reduced Voltage Stresses," *IEEE Trans. Power Electron.*, vol. 34, no. 3, pp. 2397–2404, 2019, doi: 10.1109/TPEL.2018.2842051.

[19] A. R. N. Akhormeh, K. Abbaszadeh, M. Moradzadeh, and A. Shahirinia, "High-Gain Bidirectional Quadratic DC-DC Converter Based on Coupled Inductor with Current Ripple Reduction Capability," *IEEE Trans. Ind. Electron.*, vol. 68, no. 9, pp. 7826–7837, 2021, doi: 10.1109/TIE.2020.3013551.

[20] R. G. Chougale and C. R. Lakade, "Regenerative braking system of electric vehicle driven by brushless DC motor using fuzzy logic," *IEEE Int. Conf. Power, Control. Signals Instrum. Eng. ICPCSI 2017*, vol. 61, no. 10, pp. 2167–2171, 2018, doi: 10.1109/ICPCSI.2017.8392101.

[21] F. Naseri, E. Farjah, and T. Ghanbari, "An Efficient Regenerative Braking System Based on Battery/Supercapacitor for Electric, Hybrid, and Plug-In Hybrid Electric Vehicles With BLDC Motor," *IEEE Trans. Veh. Technol.*, vol. 66, no. 5, pp. 3724–3738, 2017, doi: 10.1109/TVT.2016.2611655.

[22] K. A. Singh and K. Chaudhary, "Design and development of a new three-phase AC-DC single-stage wind energy conversion system," *IET Power Electron.*, vol. 14, no. 2, pp. 302–312, 2021, doi: https://doi.org/10.1049/pel2.12034.